JCTC Journal of Chemical Theory and Computation

Article

pubs.acs.org/JCTC

Exploring the Conical Intersection Seam: The Seam Space Nudged Elastic Band Method

Toshifumi Mori[†,‡,§] and Todd. J. Martínez*[,†,‡]

[†]PULSE Institute and Department of Chemistry, Stanford University, Stanford, California 94305, United States

[‡]SLAC National Accelerator Laboratory, 2575 Sand Hill Road, Menlo Park, California 94025, United States

Supporting Information

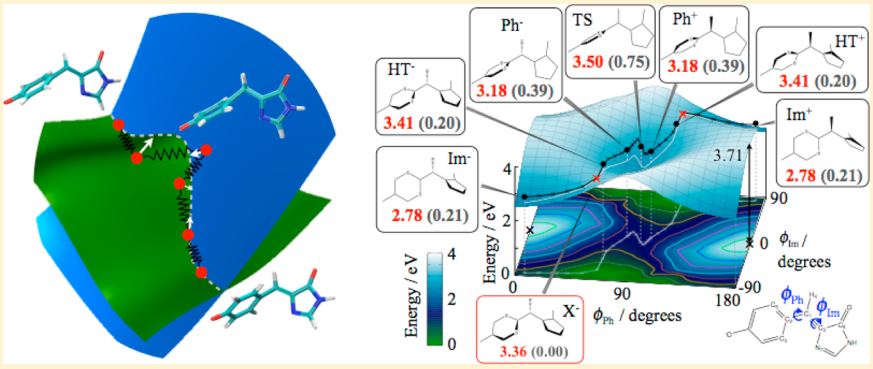

ABSTRACT: Conical intersections (CIs) play a fundamental role in photoreactions. Although it is widely known that CIs are not isolated points but rather multidimensional seams, there is a dearth of techniques to explore and characterize these seams beyond the immediate vicinity of minimum energy points within the intersection space (minimum energy conical intersections or MECIs). Here, we develop a method that connects these MECIs by minimal energy paths within the space of geometries that maintain the electronic degeneracy (the "seam space") in order to obtain a more general picture of a CI seam. This method, the seam space nudged elastic band (SS-NEB) method, combines the nudged elastic band method with gradient projected MECI optimization. It provides a very efficient way of finding minimum energy seam paths in the conical intersection seam. The method is demonstrated by application to two molecules: ethylene and the green fluorescent protein (GFP) chromophore. The results show that previously known MECIs for these molecules are connected within a single seam, adding further support to previous conjectures that all MECIs are topologically connected in the seam space. Analysis of the nonadiabatic dynamics further suggests that a broad range of seam geometries, not only the vicinity of MECIs, is involved in the nonadiabatic transition events. The current method provides a tool to characterize CI seams in different environments and to explore the importance of the seam in the dynamics.

INTRODUCTION

Conical intersections (CIs) of two or more potential energy surfaces (PESs) play a fundamental role in photochemistry.[1−8] Ultrafast processes are well-known to involve nonadiabatic transitions through CIs, e.g., photoisomerization of retinal protonated Schiff base[9−11] and radiationless deactivation of DNA bases.[12−14] Fluorescent protein chromophores also have deactivation pathways that involve CIs. These are suppressed in protein environments under fluorescent conditions[15,16] but dominate in solution[17,18] and may also be critical in the mechanisms of photoswitching proteins such as Dronpa.[19] Furthermore, efficient ground to excited state transitions can be mediated by CIs, e.g., in firefly Luciferase.[20] These studies suggest that CIs may play a role not only in ultrafast photochemical reactions but also for ground state reactions when two or more electronic states are involved.

It is well-known that CIs are not isolated points but rather $3N - 8$ dimensional seams (with N being the number of atoms). However, with a few notable exceptions (which exploited molecular symmetry and simplified reaction coordinates),[4,21−30] our knowledge of CI seams is often limited to only a few representative energy minima within the seam, known as minimum energy conical intersections (MECIs). MECIs have been found in various molecules and used to explain excited state reaction mechanisms.[10,11,13,31,32] However, it is not clear to what extent MECIs characterize or determine the dynamics of photoreactions, and indeed, dynamics simulations suggest that nonadiabatic decay may often occur at points far from MECIs.[33,34] Therefore, it is desirable to explore a wider range of geometries within CI seams and examine which parts of the seam are most important in promoting nonadiabatic transitions.

Received: October 15, 2012
Published: December 18, 2012

One approach to characterizing the set of geometries that make up the CI seam is to locate "seam paths" that connect discrete points on the CI seam (usually MECIs) while maintaining the degeneracy of two or more electronic states (i.e., remaining in the "seam space"). One of the earliest attempts[21] optimized seam paths starting from a "transition state" in the seam space and then following a steepest descent path constrained to maintain the electronic degeneracy. The "transition state" in this case is a first-order saddle point only on the manifold of geometries restricted to the seam space and thus is not a true transition state. This method requires prior knowledge of "transition state" geometries within the seam space, and such points are difficult to locate when they are not determined by symmetry. In order to address this difficulty, Sicilia et al.[35] followed a shallowest ascent path upward from an MECI geometry in order to locate a transition state in the seam space. This method requires calculation of second derivatives of the PESs (the Hessian matrix), which are then projected to remove displacements that would remove the electronic degeneracy (displacements in the branching plane). Because the branching plane directions can change rapidly along a path in the seam space, it is then necessary to carefully update the Hessian matrix at each step. Other approaches have also been attempted, e.g., to use a geometric constraint together with an MECI optimization method[23,34,36] or to apply constrained molecular dynamics methods.[37,38] Nevertheless, even the simple case of locating a seam path that connects two MECIs characterized by two coordinates (such as torsion angles) is still a challenging task.

In this work, we develop the seam space nudged elastic band (SS-NEB) method to optimize a minimum energy seam path (MESP) efficiently. We combine the nudged elastic band (NEB) method[39,40] (widely used to calculate minimum energy paths on a single PES) with a standard geometry optimization technique used to optimize MECIs.[41] Given two points lying on the CI seam (typically MECIs), the SS-NEB method locates the MESP connecting these two end points without prior knowledge of the details of the path (e.g., transition states connecting the end points). We exemplify the algorithm with S_1/S_0 CI seam paths connecting various MECIs in ethylene and the anionic form of the green fluorescent protein (GFP) chromophore. The first example demonstrates the validity of the current method and furthermore discusses the relevance of the CI seam in dynamics by comparing the MESP to geometries that promote electronic transitions in nonadiabatic dynamics simulations. The second example applies the method to a larger system that includes a concerted change of two dihedral angles about the phenyl and imidazole rings in the CI seam. These results show that previously studied MECIs are connected within the same CI seam[42] and furthermore give some insights as to what part of the CI seam may become important in the dynamics.

THEORETICAL METHOD

The PES in the vicinity of a point in the conical intersection (CI) seam is often characterized by two vectors: the energy difference gradient ($\mathbf{g}_{IJ}$) and the interstate coupling ($\mathbf{h}_{IJ}$) vectors that span the so-called branching plane (displacements which remove the degeneracy in first order). These vectors are defined as

$$\mathbf{g}_{IJ} = \frac{\partial E_I}{\partial \mathbf{R}} - \frac{\partial E_J}{\partial \mathbf{R}}$$

$$\mathbf{h}_{IJ} \simeq (E_I - E_J)\left\langle \Psi_I \middle| \frac{\partial}{\partial \mathbf{R}} \middle| \Psi_J \right\rangle \tag{1}$$

Here, I and J are the degenerate adiabatic electronic states (we take $I < J$ in the following). The remaining $3N - 8$ vibrational degrees of freedom (where N is the number of atoms in the molecule) describe the seam space. To first order, displacements in the seam space do not remove the degeneracy around a CI. Thus, the degeneracy is preserved when a small geometry displacement $\delta\mathbf{R}$ away from the CI satisfies the two conditions:[7]

$$\mathbf{g}_{IJ}\cdot\delta\mathbf{R} = 0$$

$$\mathbf{h}_{IJ}\cdot\delta\mathbf{R} = 0 \tag{2}$$

For geometries sufficiently near the CI seam, displacement along the vector $\mathbf{g}_{IJ}$ will lower the energy gap and lead to a CI.

One of the first algorithms[41] for locating MECIs was based on simultaneous minimization of (1) the energy of the upper state with respect to displacements in the seam space and (2) the energy gap with respect to displacements in the branching plane. This projected gradient approach is not restricted to optimization of MECIs but can be used quite generally to minimize any function subject to the constraint that the solution lies within the CI seam. For example, one could minimize the distance to a reference geometry, leading to a "minimal distance CI" or MDCI with respect to the chosen geometry (the closest geometry lying on the CI seam).[43,44] The basic approach is summarized for an arbitrary function $f(\mathbf{R})$, where $\mathbf{R}$ denotes the coordinates of the molecule, by defining the search direction at each step as

$$\mathbf{F}_{IJ} = \mathbf{F}_{IJ}^{\text{seam}} + \mathbf{F}_{IJ}^{\text{gap}} \tag{3}$$

where $\mathbf{F}^{\text{seam}}$ and $\mathbf{F}^{\text{gap}}$ are the gradients in the seam space and branching plane, respectively:

$$\mathbf{F}_{IJ}^{\text{seam}} = \hat{\mathcal{P}}_{IJ}^{\perp g,h}\frac{\partial f}{\partial \mathbf{R}} \tag{4}$$

$$\mathbf{F}_{IJ}^{\text{gap}} = (E_I - E_J)\mathbf{g}_{IJ} \tag{5}$$

The seam space projection operator $\hat{\mathcal{P}}_{IJ}^{\perp g,h}$ is defined as

$$\hat{\mathcal{P}}_{IJ}^{\perp g,h} \equiv \hat{\mathbf{I}} - \hat{\mathbf{x}}_g\hat{\mathbf{x}}_g^T - \hat{\mathbf{x}}_h\hat{\mathbf{x}}_h^T \tag{6}$$

$$\mathbf{x}_g = \mathbf{g}_{IJ},\ \mathbf{x}_h = \mathbf{h}_{IJ} - \mathbf{h}_{IJ}\cdot\hat{\mathbf{x}}_g \tag{7}$$

where $\hat{\mathbf{I}}$ is the identity matrix and $\hat{\mathbf{x}}$ denotes a unit vector in the direction of $\mathbf{x}$, i.e., $\hat{\mathbf{x}} = \mathbf{x}/|\mathbf{x}|$. Since $\mathbf{g}_{IJ}$ and $\mathbf{h}_{IJ}$ are not orthogonal in general, a set of orthogonalized vectors $\mathbf{x}_g$ and $\mathbf{x}_h$ are defined in eq 7. When $f(\mathbf{R})$ is the upper state potential energy, minimization following the search direction in eq 3 terminates in an MECI. Similarly, if $f(\mathbf{R})$ is the distance from a reference geometry, a minimization procedure following this search direction will give an MDCI.

This projected gradient approach is not limited to locating a single geometry. As we show below, it can be combined with reaction path search methods intended to locate minimum energy paths (MEPs) connecting reactant and product geometries. When MEP search methods are combined with

the projected gradient technique, the resulting method locates MEPs constrained to lie within the seam space, i.e., minimum energy seam paths (MESPs). In this work, we combine the projected gradient and nudged elastic band (NEB) methods, yielding the "seam-space nudged elastic band" (SS-NEB) method. The SS-NEB method can be used to locate the MESP that connects a pair of MECIs.

In the conventional NEB method, a MEP is obtained by minimizing the energy of molecular configurations (beads) distributed between two end point geometries under the constraint that each bead is connected to the neighboring bead(s) with a harmonic spring. The force on the ith bead (on state J) is given by

$$\mathbf{F}_{i,J} = \mathbf{F}_{i,J}^{\perp\tau} + \mathbf{F}_{i,J}^{\parallel\tau} \tag{8}$$

with $\mathbf{F}_{i,J}^{\perp\tau}$ and $\mathbf{F}_{i,J}^{\parallel\tau}$ being the forces perpendicular and parallel to the tangent direction of the path, respectively, defined as

$$\mathbf{F}_{i,J}^{\perp\tau} = \frac{\partial}{\partial \mathbf{R}} E_J(\mathbf{R}_i) - \left(\hat{\tau}_{i,J} \cdot \frac{\partial}{\partial \mathbf{R}} E_J(\mathbf{R}_i)\right)\hat{\tau}_{i,J} \tag{9}$$

$$\mathbf{F}_{i,J}^{\parallel\tau} = k(|\mathbf{R}_{i+1} - \mathbf{R}_i| - |\mathbf{R}_i - \mathbf{R}_{i-1}|)\hat{\tau}_{i,J} \tag{10}$$

where $\mathbf{R}_i$ is the vector of coordinates for the ith bead. Here, $\hat{\tau}_{i,J}$ is the (normalized) tangent direction of the path at point i on state J and k is the force constant of the spring connecting neighboring beads. There are a number of commonly used definitions for the spring force $\mathbf{F}_{i,J}^{\parallel\tau}$ and the tangent direction $\hat{\tau}_{i,J}$. In this work, we use eq 10 and the improved tangent formulation:[40]

$$\tau_{i,J} = \begin{cases} \tau_i^+ & \text{if} \quad E_{i+1,J} > E_{i,J} > E_{i-1,J} \\ \tau_i^- & \text{if} \quad E_{i+1,J} < E_{i,J} < E_{i-1,J} \\ \tau_i^+ \Delta E_{i,J}^{\max} + \tau_i^- \Delta E_{i,J}^{\min} & \text{if} \quad E_{i+1,J} > E_{i-1,J} > E_{i,J} \text{ or } E_{i,J} > E_{i+1,J} > E_{i-1,J} \\ \tau_i^+ \Delta E_{i,J}^{\min} + \tau_i^- \Delta E_{i,J}^{\max} & \text{if} \quad E_{i+1,J} < E_{i-1,J} < E_{i,J} \text{ or } E_{i,J} < E_{i+1,J} < E_{i-1,J} \end{cases} \tag{11}$$

where $E_{i,J} = E_J(\mathbf{R}_i)$, $\tau_i^+ = \mathbf{R}_{i+1} - \mathbf{R}_i$, $\tau_i^- = \mathbf{R}_i - \mathbf{R}_{i-1}$, $\tau_1 = \tau_1^+$, $\tau_N = \tau_N^-$ (with N being the number of beads) and

$$\Delta E_{i,J}^{\max} = \max(|E_{i+1,J} - E_{i,J}|, |E_{i-1,J} - E_{i,J}|)$$
$$\Delta E_{i,J}^{\min} = \min(|E_{i+1,J} - E_{i,J}|, |E_{i-1,J} - E_{i,J}|) \tag{12}$$

Modification of this method to optimize a MESP is achieved by realizing that a similar NEB technique can be used within the CI seam space. The tangent direction within the CI seam for bead i is given by applying the projection operator in eq 6 to the original tangent direction $\tau_{i,J}$

$$\tau_{i,IJ}^{\text{seam}} = \hat{\mathcal{P}}_{IJ}^{\perp g,h} \tau_{i,J} \tag{13}$$

and the perpendicular and spring forces are similarly constrained to act within the CI seam space. These projections give the total force on the ith bead of the SS-NEB method

$$\mathbf{F}_{i,IJ} = \hat{\mathcal{P}}_{IJ}^{\perp g,h,\tau} \mathbf{F}_{i,J} + \hat{\mathcal{P}}_{IJ}^{\perp g,h} \mathbf{F}_{i,J}^{\parallel\tau} + \mathbf{F}_{i,IJ}^{\text{gap}} \tag{14}$$

where $\mathbf{F}_{i,J}$ is the gradient of the upper (Jth) state at the ith bead and $\hat{\mathcal{P}}_{IJ}^{\perp g,h,\tau}$ is the projection operator

$$\hat{\mathcal{P}}_{IJ}^{\perp g,h,\tau} \equiv \mathbf{I} - \hat{\mathbf{x}}_g \hat{\mathbf{x}}_g^T - \hat{\mathbf{x}}_h \hat{\mathbf{x}}_h^T - \hat{\tau}_{i,IJ}^{\text{seam}} (\hat{\tau}_{i,IJ}^{\text{seam}})^T \tag{15}$$

Note that the three terms in eq 14 are orthogonal to each other. The first term in eq 14 lowers the energy of state J in the seam space (along the direction perpendicular to $\tau_{i,IJ}^{\text{seam}}$), the second term moves the bead along the local tangent direction within the seam, and the last term brings the ith bead to the seam space.

COMPUTATIONAL DETAILS

The SS-NEB method described above was applied to study the minimum energy paths within the S_1/S_0 CI seam of ethylene and a model GFP chromophore, anionic p-hydroxybenzylidene-imidazolinone (HBI). Two electrons and two active orbitals were used for the active space of ethylene, and the lowest three singlet states were averaged in the state-averaged complete active space self-consistent field (SA-CASSCF) method, i.e., SA-3-CAS(2/2). The seam path of ethylene was also located with multistate multireference second-order perturbation theory[45] (MSPT2) method using analytical nonadiabatic coupling vectors[46,47] and energy gradients,[48,49] referred to as SA-3-CAS(2/2)-MSPT2 below. The resulting MESP was used to characterize the distribution of nonadiabatic decay events in a photodynamics simulation carried out with the *ab initio* multiple spawning (AIMS) method (see Supporting Information and previous work[47] for details of the dynamics simulations). We also located and characterized the CI seam of HBI using SA-CASSCF averaged over the three lowest singlet states (S_0, S_1, S_2) with an active space consisting of four electrons in three active orbitals, i.e., SA-3-CAS(4/3). These HBI calculations are not expected to be quantitatively accurate since they do not include dynamic electron correlation effects. However, our primary purpose here is to demonstrate the applicability of the SS-NEB method and to provide a qualitative picture of the connectivity of MECIs in HBI.[50,51] The 6-31G* basis set was used in all reported calculations. The end points of MESPs (i.e., MECIs) were optimized before the SS-NEB calculation. The SS-NEB calculations used 11 beads, and the corresponding initial molecular geometries were generated by linear interpolation (in either Cartesian or internal coordinates) between the MECI end points. Geometries in each step of the SS-NEB calculation were updated using the conjugate gradient method implemented in the DL-FIND code.[52] Electronic structure calculations and MECI optimizations were performed with the MOLPRO 2006 program package[53] with our modifications to calculate the analytic MSPT2 nonadiabatic coupling and the DL-FIND code[52] was modified to carry out SS-NEB calculations.

RESULTS AND DISCUSSION

Ethylene. Ethylene has been widely studied as a prototype for photoinduced *cis*−*trans* isomerization reactions.[23,47,54−65] Two distinct classes of S_1/S_0 MECIs have been implicated in

the photoisomerization mechanism—the first of these is characterized by torsion about the C=C bond and pyramidalization about one of the C atoms (referred to as "twisted-pyramidalized" or CI_{TwPy}), while the second is characterized by an ethylidene-like arrangement ($HCCH_3$) of the atoms (referred to as the "ethylidene" CI or CI_{Et}). There are numerous symmetry-equivalent geometries for both of these MECIs. For example, in the CI_{TwPy} geometry, the left or the right C atom can be pyramidalized, and the pyramidalization can be above or below the CCH_2 plane. Seam space paths connecting these two MECIs and/or symmetry-equivalent variants of the same MECI have been discussed previously,[23,38,66,67] primarily using CASSCF methods. In this work, we use the SS-NEB method to calculate MESPs using both the CASSCF and MSPT2 methods, highlighting the effect of dynamic electron correlation on the MESP. In Figure 1, we

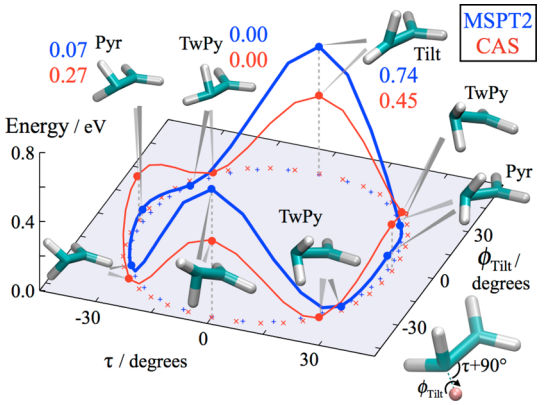

Figure 1. S_1/S_0 seam path connecting symmetry-equivalent variants of the twisted/pyramidalized MECI (CI_{TwPy}) in ethylene as a function of pyramidalization and tilt angles (see inset; detailed definitions of these angles are available in Supporting Information). Geometries and energies (in eV, with the zero of energy corresponding to the CI_{TwPy} geometry) at characteristic points are also shown. MESPs are optimized with CASSCF (red) and MSPT2 (blue).

show the resulting MESP that connects the symmetry-equivalent CI_{TwPy} geometries. Even when we restrict the considered geometries such that the same C atom is pyramidalized, there are four symmetry-equivalent MECIs—this is because of the two senses of pyramidalization and furthermore that one of the H atoms bonded to the pyramidalized C atom has a longer C−H bond length (corresponding to a "tilting" of the pyramidalized CH_2 group and partial migration of the H atom toward the ethylidene geometry). The MESPs from CASSCF and MSPT2 are qualitatively similar, but the relative energies of the "seam space transition states" are quite different. Compared to the CASSCF MESP, the MSPT2 seam space path is much flatter with respect to the tilting of the pyramidalized methylene unit and at the same time much more strongly favors pyramidalization of the methylene. Although we show only the tilt and pyramidalization angles in Figure 1, all coordinates are optimized, and further details of other geometric parameters (coordinate definitions and values along the MESP) are given in the Supporting Information.

In Figure 2, we show the MESP that connects the twisted-pyramidalized MECI with the ethylidene MECI. The effect of dynamic electron correlation is much more pronounced here, with CASSCF predicting that the MECI corresponding to

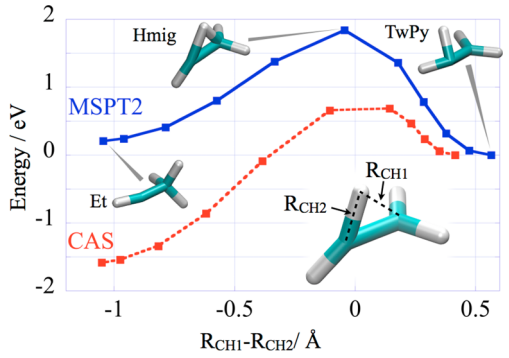

Figure 2. Energies along the S_1/S_0 seam path connecting $(Et)_{CI}$ and $(TwPy)_{CI}$ MECI geometries of ethylene, plotted as a function of H migration distance (defined as the difference of the two CH distances R_{CH1} and R_{CH2} shown in the inset). MSPT2 and CASSCF-optimized paths are shown in blue and red, respectively.

ethylidene (CI_{Et}) is more stable than the twisted/pyramidalized MECI (CI_{TwPy}). Including dynamic electron correlation effects significantly raises the "seam space barrier" between the CI_{TwPy} and CI_{Et} structures and also destabilizes the CI_{Et} structure substantially. This is consistent with results from dynamics simulations, where the formation of ethylidene is much more prevalent when CASSCF PESs are used, compared to dynamics on MSPT2 PESs.[3,23,47,68,69]

All of the geometries along the seam paths shown in Figures 1 and 2 are well below the vertical excitation energy, which is 3.92 and 3.09 eV above the energy of CI_{TwPy} for CASSCF and MSPT2 methods, respectively. All of the geometries along these MESPs are thus energetically accessible after photoexcitation. This makes it interesting to ask whether any regions of the MESP are more "active" in nonadiabatic transitions than others. We answer this question using AIMS simulations of the excited state dynamics, exciting the molecule to the bright $\pi\pi^*$ state (S_1) and calculating the PESs and couplings during the dynamics with CASSCF or MSPT2, as described previously.[58] For each nonadiabatic transition observed in the dynamics ("spawning" of a new trajectory basis function or TBF), we located the nearest point along the MESPs determined above (distance being measured by the root-mean-squared deviation or RMSD of the spawning geometry and geometries along the MESP). The population transferred through each spawning event (determined by solving the time-dependent Schrödinger equation in the basis of TBFs) was then assigned to this nearest geometry along the MESP as

$$\Delta P_{S_1\to S_0}(i) = \int dt \sum_m \Delta P_{S_1\to S_0}(\bar{\mathbf{R}}_m(t)) \times \delta(i, \arg\min_j |\bar{\mathbf{R}}_m(t) - \mathbf{R}_j|) \quad (16)$$

Here, $\Delta P_{S_1\to S_0}(i)$ is the population transferred from S_1 to S_0 due to spawning events closest to the ith bead along the MESP, m indexes the parent trajectory basis functions (TBF), $\bar{\mathbf{R}}_m(t)$ and $\mathbf{R}_j$ are the nuclear coordinates of the mth TBF at time t and jth point along the MESP, respectively, and $\Delta P_{S_1\to S_0}(\bar{\mathbf{R}}_m(t))$ is the amount of population transferred (from S_1 to S_0) from the parent TBF m at time t. The fraction of the population transferred from S_1 to S_0 through each point along the MESP (i.e., $\Delta P_{S_1\to S_0}(i)/\sum_j \Delta P_{S_1\to S_0}(j)$) is plotted in Figure 3. The graph shows that, for MSPT2 dynamics, most of the

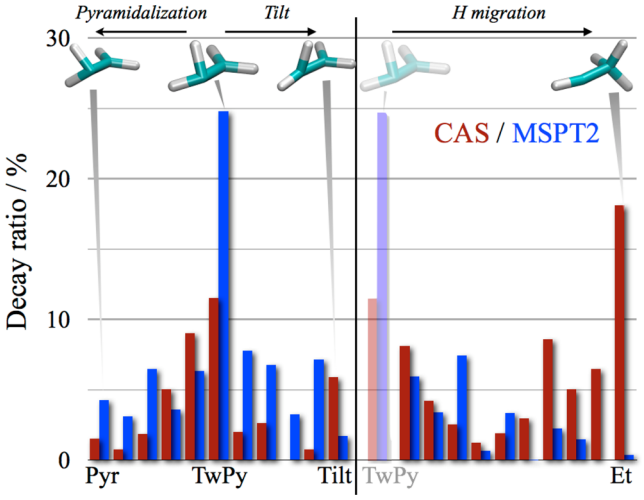

Figure 3. Population transfer from S_1 to S_0 as a function of the nearest point along the CI seam paths shown in Figures 1 (left half of plot) and 2 (right half of plot). Nonadiabatic decay events in each time step during the AIMS dynamics were assigned to the point along MESPs with the closest geometry as defined by root-mean-square-distance. Only a quarter of the MESP from Figure 1 is plotted as rest is symmetrically equivalent, and the transparent bar on the right indicates that this geometry corresponds to the bar labeled TwPy on the left side of the plot. CASSCF and MSPT2 results are shown in red and blue, respectively. In each case, the dynamics and MESP are calculated at the same level of theory (i.e., CASSCF or MSPT2).

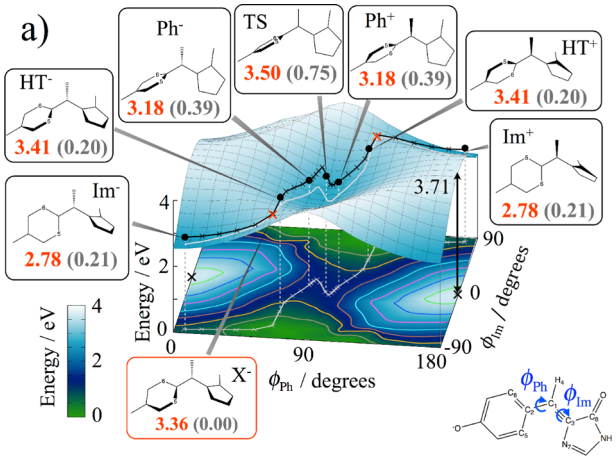

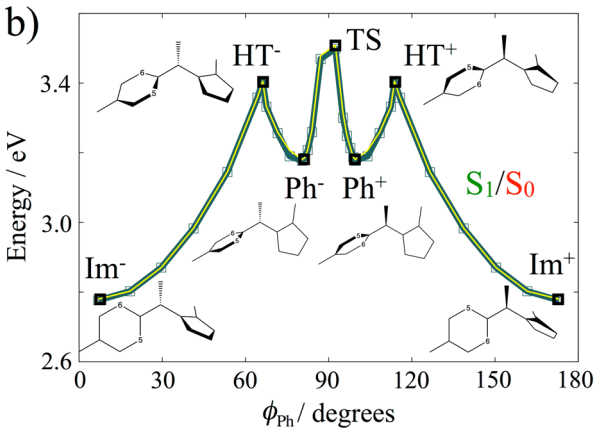

Figure 4. (a) The S_1/S_0 MESP and S_1 state PES of HBI as a function of the dihedral angles ϕ_{Ph} and ϕ_{Im} (defined in the inset at the lower right). The MESP is plotted as a black line, the surface represents the S_1 PES (S_1 energy is minimized while constraining the ϕ_{Ph} and ϕ_{Im} torsion angles), and the energy difference between S_1 and S_0 states at each of these geometries in the S_1 PES is shown as a contour plot below. The MESP connects the Im^- and Im^+ MECI geometries, passing through the Ph^- and Ph^+ MECIs. Black crosses represent the optimized bead points along the MESP. The projection of the MESP onto the S_1 state PES, i.e., a path with geometries having the same ϕ_{Ph} and ϕ_{Im} torsion angles as the MESP, is shown on the surface and contour plots as a white line. The geometries of structures along the MESP are shown in boxes. The energy (in eV) of each of these geometries relative to the S_0 energy at a planar-constrained minimum on S_1 (this planar-constrained minimum is indicated with black ×'s) is shown in red text. The energy difference between the MESP and projected path geometries is shown in gray text within parentheses. The geometries where the MESP is the lowest point on S_1 for the given ϕ_{Ph} and ϕ_{Im} torsion angles are labeled X^- and X^+, and these are indicated on the surface plot with red x's. Detailed definitions of ϕ_{Ph} and ϕ_{Im} can be found in the Supporting Information (Figure S3). (b) S_1/S_0 MESP as a function of ϕ_{Ph}. The energies of S_1 and S_0 states are shown in yellow and green, respectively, and minima and transition states are marked with black boxes.

nonadiabatic transitions take place in the vicinity of CI_{TwPy}. In contrast, for CASSCF dynamics, nonadiabatic transitions are observed with similar frequency in the vicinity of both CI_{TwPy} and CI_{Et}. This finding is consistent with previous AIMS dynamics results[47,68,70] and indicates that the energetic placement of MECIs does affect nonadiabatic decay efficiency. However, in both MSPT2 and CASSCF dynamics, more than 70% of the nonadiabatic population transfer occurs in the vicinity of points other than MECIs, emphasizing the importance of large portions of the CI seam in nonadiabatic dynamics.

Green Fluorescent Protein Chromophore. To show the applicability of the current method to larger molecules, we explored the S_1/S_0 CI seam of the anionic HBI. The HBI molecule is known to undergo ultrafast nonradiative transitions to the ground state after excitation in solution[17,18] and also in some protein environments.[19] In contrast, the molecule is highly fluorescent in most protein environments,[15,16] implying that the protein environment prevents nonradiative transitions. The isolated HBI molecule is known to have two S_1/S_0 MECIs, involving torsion of the phenyl or imidazole rings about the adjacent C−C bond in the bridging unit connecting the two rings. Hereafter, we denote these two MECIs as CI_{Ph} and CI_{Im}, respectively. Additionally, a so-called "*hula-twist*" CI,[71] where the two rings twist simultaneously, has also been discussed as a "volume-conserving" CI that could be important in photodynamics occurring in the sterically constrained protein environment. Here, we calculated the MESP connecting CI_{Im} and CI_{Ph}, considering both senses of torsion for the phenyl and imidazole rings. The result is shown as a black line in Figure 4, where the direction of torsion for the rings is denoted as "−" and "+". For the isolated HBI molecule, the direction of the torsion does not affect the energy; i.e., CI_{Ph+} and CI_{Ph-} are symmetry-equivalent (and likewise for CI_{Im+} and CI_{Im-}). Figure 4 also shows the S_1 PES (surface plot) as a function of the two dihedral angles ϕ_{Ph} and ϕ_{Im} (the geometry is optimized to minimize the S_1 energy subject to constraints on the ϕ_{Ph} and ϕ_{Im} dihedral angles), and the S_1/S_0 energy gap at these torsion-constrained S_1 energy-minimized structures is shown as a contour plot. Further details including geometric parameters can be found in Figure S3 of the Supporting Information. As

dx.doi.org/10.1021/ct300892t | J. Chem. Theory Comput. 2013, 9, 1155−1163

can be seen in Figure 4, CI_{Im} and CI_{Ph} are minima along a single MESP, connected by a "hula-twist" type intersection (denoted as HT^+ and HT^-) that forms a "transition state" in the seam space. There is a second transition state-like structure within the MESP (denoted as TS in Figure 4), connecting symmetry-equivalent MECIs (CI_{Ph+} and CI_{Ph-}). At this level of electronic structure theory, the energies of all depicted points along the MESP are below the S_1 energy at the Franck−Condon point (and even below the S_1 energy corresponding to an HBI molecule optimized on S_1 subject to a planarity constraint). Thus, all points on the MESP shown in Figure 4 could potentially play a role in the photodynamics of HBI. In addition to the MESP (black line), Figure 4 also shows the projection of the MESP on the torsion-constrained S_1 minimum energy PES (white line). Where the black and white lines coincide, the lowest energy point on S_1 with the depicted values of ϕ_{Ph} and ϕ_{Im} lies on the conical intersection seam. These geometries are labeled X^+ and X^-, and they have pronounced hula-twist character. When only one of the rings is twisted, the MESP lies above the lowest energy point on S_1. Thus, when only one of the rings is twisted in HBI, the molecule can exist in a minimum on S_1. In contrast, if both rings are twisted (the "hula-twist" geometry), the molecule will access the CI seam and nonradiative decay is likely. This may be an important consideration for the photodynamics of HBI in protein environments.

More quantitative information about the CI seam in HBI would require higher level electronic structure theory, including dynamic electron correlation.[43,46] Since our primary goal here is to demonstrate the SS-NEB method, we do not optimize the MESP at the MSPT2 level which includes both static and dynamic electron correlation. One might be tempted to calculate MSPT2 energy corrections along the MESP determined at the CASSCF level. This type of correction has been christened CASPT2//CASSCF in previous work.[27−30,72] It is worth mentioning that this procedure is ill-advised in the case of an MESP, because the degeneracy of the CASSCF states leads to an arbitrariness in the eigenvectors. It is not sufficient to use MSPT2 for such corrections, but instead one needs to use the extended multiconfigurational perturbation methods[49,72] (e.g., XMSPT2) which choose a zeroth-order Hamiltonian that resolves the ambiguous rotations between states at CASSCF degeneracies. We will investigate the reliability of such correction procedures for the MESP in future work.

SUMMARY

We have introduced constraints in the nudged elastic band (NEB) method to extend it beyond the location of minimal energy paths on a single PES. The resulting seam space nudged elastic band (SS-NEB) method locates minimum energy seam paths (MESPs) within the seam of conical intersections where two (or more) electronic states are degenerate. This method combines the gradient projection technique[41] used for minimal energy conical intersection (MECI) searches with the traditional NEB method in order to locate minimal energy paths confined to the intersection seam that connect two conical intersections (these end points are usually envisioned to be chosen as MECIs). The SS-NEB method searches for the MESP by simultaneously minimizing the energy gap, the energy along the local tangent of the path in the seam space, and the energy of the upper state in the direction perpendicular to the local tangent but within the seam space. This method does not require detailed initial knowledge of the path except for the two end points (typically MECIs), and the initial points chosen as a guess for the MESP do not need to lie within the CI seam. As in all NEB-type methods, the Hessian matrix does not need to be computed or stored, and the method is trivially parallelizable over all the beads used to describe the path.

The SS-NEB method was applied to locate MESPs in the S_1/S_0 CI seams of ethylene and HBI. For ethylene, we demonstrated the validity of the method and its applicability using both CASSCF and MSPT2 electronic structure methods. We used the MESP to characterize the portions of the PES that play the most prominent role in nonadiabatic transitions during the excited state dynamics of ethylene (using previous *ab initio* nonadiabatic dynamics results[58]). We showed that nonadiabatic transitions are not localized around the MECIs, but instead a large portion of the MESP is involved in these transitions. We also applied the SS-NEB method to the HBI anion, a model of the green fluorescent protein (GFP) chromophore. This demonstrates that the SS-NEB method can be applied to larger molecules, and we see no reason why it cannot be applied in any case where MECI searches are feasible. We located a series of "hula-twist" CIs along the MESP connecting the imidazole- and phenyl-twisted MECIs (CI_{Im} and CI_{Ph}). These "hula-twist" CIs are energetically accessible after excitation to the lowest bright excited state and may play a role in nonradiative transitions in this molecule. These are not MECIs (at least at the current level of theory) and thus would be difficult to characterize without a method that can locate MESPs.

Locating energetically accessible MESPs may open new avenues to understanding the nonadiabatic processes in photochemical reactions. While most previous PES studies have focused on MECIs to explain nonadiabatic decay mechanisms, dynamics calculations indicate that MECIs are not always relevant to the decay events;[33,34] i.e., large regions of the intersection seam can be effective in promoting nonadiabatic transitions. Our work here also supports this viewpoint. The extensive involvement of different regions of the intersection space motivates the development of general tools such as SS-NEB in order to better characterize the intersection seam. Given the ability to characterize the CI seam space, the next question is understanding what factors determine the importance of different parts of the seam in the context of nonadiabatic dynamics. Progress can be made in developing this understanding by analyzing dynamics results in light of MESPs, similar to what we did here with ethylene.

Although the current work focused on the CI seam in the gas phase, many interesting (ultrafast) photoreactions occur in solution and in protein environments. The effect of the environment on the CI seam can be dramatic.[73−79] From a static viewpoint, the intersection space can change its shape and energy; i.e., the MESPs can change and the energetics along these can be modified. From a dynamic viewpoint, the increased energy dissipation due to interactions with the solvent may increase the importance of lower energy portions of the intersection space, i.e. MESPs. The current SS-NEB method can directly be applied to existing MECI optimization methods in solution[78,80−83] and will be a powerful tool to gain insight into excited state dynamics in complex environments.

■ ASSOCIATED CONTENT

Supporting Information

Detailed descriptions of the coordinates used, more extensive descriptions of the MESPs for both ethylene and HBI, and coordinates for important points along the MESPs are available free of charge via the Internet at http://pubs.acs.org.

■ AUTHOR INFORMATION

Corresponding Author

*E-mail: todd.martinez@stanford.edu.

Present Address

[§]Department of Chemistry, University of Wisconsin, Madison, WI

Notes

The authors declare no competing financial interest.

■ ACKNOWLEDGMENTS

We thank L. D. Cremar and C. Evenhuis for helpful discussions and W. J. Glover for carefully reading and commenting on the manuscript. This work was supported by the Department of Energy under DOE Contract No. DE-AC02-7600515.

■ REFERENCES

(1) Domcke, W.; Yarkony, D.; Koppel, H. *Conical Intersections: Electronic Structure, Dynamics & Spectroscopy*; World Scientific: Singapore, 2004; p 1ff.

(2) Klessinger, M.; Michl, J. *Excited States and Photo-Chemistry of Organic Molecules*; John Wiley & Sons: New York, 1995; p 1ff.

(3) Levine, B. G.; Martínez, T. J. Isomerization through conical intersections. *Annu. Rev. Phys. Chem.* **2007**, *58*, 613−634.

(4) Yarkony, D. R. Conical Intersections: Diabolical and Often Misunderstood. *Acc. Chem. Res.* **1998**, *31*, 511−518.

(5) Sobolewski, A. L.; Domcke, W.; Dedonder-Lardeux, C.; Jouvet, C. Excited-state hydrogen detachment and hydrogen transfer driven by repulsive $1\pi\sigma^*$ states: A new paradigm for nonradiative decay in aromatic biomolecules. *Phys. Chem. Chem. Phys.* **2002**, *4*, 1093−1100.

(6) Atchity, G. J.; Xantheas, S. S.; Ruedenberg, K. Potential energy surfaces near intersections. *J. Chem. Phys.* **1991**, *95*, 1862−1876.

(7) Yarkony, D. R. Nonadiabatic quantum chemistry–past, present, and future. *Chem. Rev.* **2012**, *112*, 481−498.

(8) Sampedro Ruiz, D.; Cembran, A.; Garavelli, M.; Olivucci, M.; Fuß, W. Structure of the Conical Intersections Driving the cis−trans Photoisomerization of Conjugated Molecules. *Photochem. Photobiol.* **2002**, *76*, 622−633.

(9) Schoenlein, R. W.; Peteanu, L. A.; Mathies, R. A.; Shank, C. V. The first step in vision: femtosecond isomerization of rhodopsin. *Science* **1991**, *254*, 412−415.

(10) González-Luque, R.; Garavelli, M.; Bernardi, F.; Merchán, M.; Robb, M.; Olivucci, M. Computational evidence in favor of a two-state, two-mode model of the retinal chromophore photoisomerization. *Proc. Natl. Acad. Sci. U. S. A.* **2000**, *97*, 9379−9384.

(11) Ben-Nun, M.; Molnar, F.; Schulten, K.; Martínez, T. J. The role of intersection topography in bond selectivity of cis-trans photoisomerization. *Proc. Natl. Acad. Sci. U. S. A.* **2002**, *99*, 1769−1773.

(12) Crespo-Hernández, C. E.; Cohen, B.; Hare, P. M.; Kohler, B. Ultrafast Excited-State Dynamics in Nucleic Acids. *Chem. Rev.* **2004**, *104*, 1977−2020.

(13) Perun, S.; Sobolewski, A. L.; Domcke, W. Conical Intersections in Thymine. *J. Phys. Chem. A* **2006**, *110*, 13238−13244.

(14) Matsika, S. Three-State Conical Intersections in Nucleic Acid Bases. *J. Phys. Chem. A* **2005**, *109*, 7538−7545.

(15) Tsien, R. Y. The green fluorescent protein. *Annu. Rev. Biochem.* **1998**, *67*, 509−544.

(16) Meech, S. R. Excited state reactions in fluorescent proteins. *Chem. Soc. Rev.* **2009**, *38*, 2922−2934.

(17) Usman, A.; Mohammed, O. F.; Nibbering, E. T. J.; Dong, J.; Solntsev, K. M.; Tolbert, L. M. Excited-state structure determination of the green fluorescent protein chromophore. *J. Am. Chem. Soc.* **2005**, *127*, 11214−11215.

(18) Mandal, D.; Tahara, T.; Meech, S. R. Excited-state dynamics in the green fluorescent protein chromophore. *J. Phys. Chem. B* **2004**, *108*, 1102−1108.

(19) Ando, R.; Mizuno, H.; Miyawaki, A. Regulated fast nucleocytoplasmic shuttling observed by reversible protein highlighting. *Science* **2004**, *306*, 1370−1373.

(20) Chung, L. W.; Hayashi, S.; Lundberg, M.; Nakatsu, T.; Kato, H.; Morokuma, K. Mechanism of efficient firefly bioluminescence via adiabatic transition state and seam of sloped conical intersection. *J. Am. Chem. Soc.* **2008**, *130*, 12880−12881.

(21) Garavelli, M.; Page, C. S.; Celani, P.; Olivucci, M.; Schmid, W. E.; Trushin, S. A.; Fuss, W. Reaction Path of a sub-200 fs Photochemical Electrocyclic Reaction. *J. Phys. Chem. A* **2001**, *105*, 4458−4469.

(22) Paterson, M. J.; Bearpark, M. J.; Robb, M. A.; Blancafort, L. The curvature of the conical intersection seam: an approximate second-order analysis. *J. Chem. Phys.* **2004**, *121*, 11562−11571.

(23) Barbatti, M.; Paier, J.; Lischka, H. Photochemistry of ethylene: a multireference configuration interaction investigation of the excited-state energy surfaces. *J. Chem. Phys.* **2004**, *121*, 11614−11624.

(24) Bearpark, M. J.; Blancafort, L.; Paterson, M. J. Mapping the intersection space of the ground and first excited states of fulvene. *Mol. Phys.* **2006**, *104*, 1033−1038.

(25) Migani, A.; Robb, M. A.; Olivucci, M. Relationship between photoisomerization path and intersection space in a retinal chromophore model. *J. Am. Chem. Soc.* **2003**, *125*, 2804−2808.

(26) Kistler, K. A.; Matsika, S. Three-state conical intersections in cytosine and pyrimidinone bases. *J. Chem. Phys.* **2008**, *128*, 215102.

(27) Migani, A.; Blancafort, L.; Robb, M. A.; Debellis, A. D. An extended conical intersection seam associated with a manifold of decay paths: Excited-state intramolecular proton transfer in O-hydroxybenzaldehyde. *J. Am. Chem. Soc.* **2008**, *130*, 6932−6933.

(28) Quansong, L.; Mendive-Tapia, D.; Paterson, M. J.; Migani, A.; Bearpark, M. J.; Robb, M. A.; Blancafort, L. A global picture of the S1/S0 conical intersection seam of benzene. *Chem. Phys.* **2010**, *377*, 60−65.

(29) Li, Q.; Migani, A.; Blancafort, L. Wave Packet Dynamics at an Extended Seam of Conical Intersection: Mechanism of the Light-Induced Wolff Rearrangement. *J. Phys. Chem. Lett.* **2012**, *3*, 1056−1061.

(30) Cembran, A.; Bernardi, F.; Garavelli, M.; Gagliardi, L.; Orlandi, G. On the mechanism of the cis-trans isomerization in the lowest electronic states of azobenzene: S-0, S-1, and T-1. *J. Am. Chem. Soc.* **2004**, *126*, 3234−3243.

(31) Martin, M. E.; Negri, F.; Olivucci, M. Origin, nature, and fate of the fluorescent state of the green fluorescent protein chromophore at the CASPT2//CASSCF resolution. *J. Am. Chem. Soc.* **2004**, *126*, 5452−5464.

(32) Polyakov, I. V.; Grigorenko, B. L.; Epifanovsky, E. M.; Krylov, A. I.; Nemukhin, A. V. Potential Energy Landscape of the Electronic States of the GFP Chromophore in Different Protonation Forms: Electronic Transition Energies and Conical Intersections. *J. Chem. Theory Comput.* **2010**, *6*, 2377−2387.

(33) Hunt, P. A.; Robb, M. A. Systematic control of photochemistry: the dynamics of photoisomerization of a model cyanine dye. *J. Am. Chem. Soc.* **2005**, *127*, 5720−5726.

(34) Coe, J. D.; Ong, M. T.; Levine, B. G.; Martínez, T. J. On the Extent and Connectivity of Conical Intersection Seams and the Effects of Three-State Intersections. *J. Phys. Chem. A* **2008**, *112*, 12559−12567.

(35) Sicilia, F.; Blancafort, L.; Bearpark, M.; Robb, M. New Algorithms for Optimizing and Linking Conical Intersection Points. *J. Chem. Theory Comput.* **2008**, *4*, 257−266.

(36) Maeda, S.; Ohno, K.; Morokuma, K. Updated Branching Plane for Finding Conical Intersections without Coupling Derivative Vectors. *J. Chem. Theory Comput.* **2010**, *6*, 1538−1545.
(37) Ogihara, Y.; Yamamoto, T.; Kato, S. Ab Initio Trajectory Study on Triplet Ketene Photodissociation via Statistical Sampling of the Crossing Seam. *J. Chem. Theory Comput.* **2011**, *7*, 2507−2519.
(38) Laino, T.; Passerone, D. Pseudo-dynamics and band optimizations: shedding light into conical intersection seams. *Chem. Phys. Lett.* **2004**, *389*, 1−6.
(39) Henkelman, G.; Uberuaga, B.; Jónsson, H. A climbing image nudged elastic band method for finding saddle points and minimum energy paths. *J. Chem. Phys.* **2000**, *113*, 9901−9904.
(40) Henkelman, G.; Jónsson, H. Improved tangent estimate in the nudged elastic band method for finding minimum energy paths and saddle points. *J. Chem. Phys.* **2000**, *113*, 9978−9985.
(41) Bearpark, M.; Robb, M.; Bernhard Schlegel, H. A direct method for the location of the lowest energy point on a potential surface crossing. *Chem. Phys. Lett.* **1994**, *223*, 269−274.
(42) Martinez, T. J. General Discussion. *Faraday Disc.* **2004**, *127*, 248−249.
(43) Levine, B.; Coe, J.; Martinez, T. Optimizing Conical Intersections without Derivative Coupling Vectors: Application to Multistate Multireference Second-Order Perturbation Theory (MS-CASPT2). *J. Phys. Chem. B* **2008**, *112*, 405−413.
(44) De Vico, L.; Olivucci, M.; Lindh, R. New General Tools for Constrained Geometry Optimizations. *J. Chem. Theory Comput.* **2005**, *1*, 1029−1037.
(45) Finley, J.; Malmqvist, P.; Roos, B.; Serrano-Andrés, L. The multi-state CASPT2 method. *Chem. Phys. Lett.* **1998**, *288*, 299−306.
(46) Mori, T.; Kato, S. Dynamic electron correlation effect on conical intersections in photochemical ring-opening reaction of cyclohexadiene: MS-CASPT2 study. *Chem. Phys. Lett.* **2009**, *476*, 97−100.
(47) Mori, T.; Glover, W. J.; Schuurman, M. S.; Martínez, T. J. Role of Rydberg States in the Photochemical Dynamics of Ethylene. *J. Phys. Chem. A* **2012**, *116*, 2808−2818.
(48) Celani, P.; Werner, H. Analytical energy gradients for internally contracted second-order multireference perturbation theory. *J. Chem. Phys.* **2003**, *119*, 5044.
(49) Shiozaki, T.; Gyorffy, W.; Celani, P.; Werner, H.-J. Extended multi-state complete active space second-order perturbation theory: Energy and nuclear gradients. *J. Chem. Phys.* **2011**, *135*, 081106.
(50) Olsen, S.; McKenzie, R. H. A diabatic three-state representation of photoisomerization in the green fluorescent protein chromophore. *J. Chem. Phys.* **2009**, *130*, 184302.
(51) Olsen, S.; Smith, S. C. Bond selection in the photoisomerization reaction of anionic green fluorescent protein and kindling fluorescent protein chromophore models. *J. Am. Chem. Soc.* **2008**, *130*, 8677−8689.
(52) Kastner, J.; Carr, J. M.; Keal, T. W.; Thiel, W.; Wander, A.; Sherwood, P. DL-FIND: An Open-Source Geometry Optimizer for Atomistic Simulations. *J. Phys. Chem. A* **2009**, *113*, 11856−11865.
(53) Werner, H.-J.; Knowles, P. J.; Lindh, R.; Manby, F. R.; Schutz, M.; Celani, P.; Korona, T.; Rauhut, G.; Amos, R. D.; Bernhardsson, A.; Berning, A.; Cooper, D. L.; Deegan, M. J. O.; Dobbyn, A. J.; Eckert, F.; Hampel, C.; Hetzer, G.; Lloyd, A. W.; McNicholas, S. J.; Meyer, W.; Mura, M. E.; Nicklass, A.; Palmieri, P.; Pitzer, R.; Schumann, U.; Stoll, H.; Stone, A. J.; Tarroni, R.; Thorsteinsson, T. *MOLPRO*, version 2006.1; Institut für Theoretische Chemie, Universität Stuttgart: Stuttgart, Germany, 2006.
(54) Ohmine, I. Mechanisms of nonadiabatic transitions in photoisomerization processes of conjugated molecules: Role of hydrogen migrations. *J. Chem. Phys.* **1985**, *83*, 2348−2362.
(55) Quenneville, J.; Ben-Nun, M.; Martinez, T. J. Photochemistry from first principles - advances and future prospects. *J. Photochem. Photobiol. A* **2001**, *144*, 229−235.
(56) Viel, A.; Krawczyk, R. P.; Manthe, U.; Domcke, W. Photoinduced dynamics of ethene in the N, V, and Z valence states: A six-dimensional nonadiabatic quantum dynamics investigation. *J. Chem. Phys.* **2004**, *120*, 11000−11010.
(57) Stert, V.; Lippert, H.; Ritze, H.; Radloff, W. Femtosecond time-resolved dynamics of the electronically excited ethylene molecule. *Chem. Phys. Lett.* **2004**, *388*, 144−149.
(58) Tao, H.; Allison, T. K.; Wright, T. W.; Stooke, A. M.; Khurmi, C.; van Tilborg, J.; Liu, Y.; Falcone, R. W.; Belkacem, A.; Martínez, T. J. Ultrafast internal conversion in ethylene. I. The excited state lifetime. *J. Chem. Phys.* **2011**, *134*, 244306.
(59) Cromwell, E. F.; Stolow, A.; Vrakking, M. J. J.; Lee, Y. T. Dynamics of ethylene photodissociation from rovibrational and translational energy distributions of H_2 products. *J. Chem. Phys.* **1992**, *97*, 4029−4040.
(60) Farmanara, P.; Stert, V.; Radloff, S. Ultrafast internal conversion and fragmentation in electronically excited C2H4 and C2H3Cl molecules. *Chem. Phys. Lett.* **1998**, *288*, 518−522.
(61) Mestdagh, J.-M.; Visticot, J.-P.; Elhanine, M.; Soep, B. Prereactive evolution of monoalkenes excited in the 6 eV region. *J. Chem. Phys.* **2000**, *113*, 237−248.
(62) Lin, J. J.; Wang, C. C.; Lee, Y. T.; Yang, X. Site-specific dissociation dynamics of ethylene at 157nm: Atomic and molecular hydrogen elimination. *J. Chem. Phys.* **2000**, *113*, 9668−9677.
(63) Lee, S.-H.; Lee, Y. T.; Yang, X. Dynamics of photodissociation of ethylene and its isotopomers at 157nm: Branching rations and kinetic energy distributions. *J. Chem. Phys.* **2004**, *120*, 10983−10991.
(64) Kosma, K.; Trushin, S.; Fuss, W.; Schmid, W. Ultrafast dynamics and coherent oscillations in ethylene and ethylene-d4 excited at 162 nm. *J. Phys. Chem. A* **2008**, *112*, 7514−7529.
(65) Ben-Nun, M.; Martínez, T. Ab initio molecular dynamics study of cis-trans photoisomerization in ethylene. *Chem. Phys. Lett.* **1998**, *298*, 57−65.
(66) Wilsey, S.; Houk, K. N. H/Vinyl and Alkyl/Vinyl Conical Intersections Leading to Carbene Formation from the Excited States of Cyclohexene and Norbornene. *J. Am. Chem. Soc.* **2002**, *124*, 11182−11190.
(67) Ben-Nun, M.; Martinez, T. J. Photodynamics of ethylene: ab initio studies of conical intersections. *Chem. Phys.* **2000**, *259*, 237−248.
(68) Tao, H.; Levine, B.; Martinez, T. Ab Initio Multiple Spawning Dynamics Using Multi-State Second-Order Perturbation Theory. *J. Phys. Chem. A* **2009**, *113*, 13656−13662.
(69) Virshup, A.; Chen, J.; Martinez, T. J. Nonlinear dimensionality reduction for nonadiabatic dynamics: The influence of conincal intersection topography on population transfer rates. *J. Chem. Phys.* **2012**, *137*, 22A519.
(70) Levine, B.; Coe, J.; Virshup, A.; Martínez, T. Implementation of ab initio multiple spawning in the Molpro quantum chemistry package. *Chem. Phys.* **2008**, *347*, 3−16.
(71) Weber, W.; Helms, V.; McCammon, J. A.; Langhoff, P. W. Shedding light on the dark and weakly fluorescent states of green fluorescent proteins. *Proc. Natl. Acad. Sci. U. S. A.* **1999**, *96*, 6177−6182.
(72) Granovsky, A. A. Extended multi-configuration quasi-degenerate perturbation theory: the new approach to multi-state multi-reference perturbation theory. *J. Chem. Phys.* **2011**, *134*, 214113.
(73) Yamazaki, S.; Kato, S. Solvent Effect on Conical Intersections in Excited-State 9H-Adenine: Radiationless Decay Mechanism in Polar Solvent. *J. Am. Chem. Soc.* **2007**, *129*, 2901−2909.
(74) Burghardt, I.; Cederbaum, L. S.; Hynes, J. T. Environmental effects on a conical intersection: A model study. *Faraday Discuss.* **2004**, *127*, 395−411.
(75) Spezia, R.; Burghardt, I.; Hynes, J. T. Conical intersections in solution: non-equilibrium versus equilibrium solvation. *Mol. Phys.* **2006**, *104*, 903−914.
(76) Malhado, J. P.; Spezia, R.; Hynes, J. T. Dynamical friction effects on the photoisomerization of a model protonated Schiff base in solution. *J. Phys. Chem. A* **2011**, *115*, 3720−3735.
(77) Virshup, A. M.; Punwong, C.; Pogorelov, T. V.; Lindquist, B. A.; Ko, C.; Martinez, T. J. Photodynamics in complex environments: ab initio multiple spawning quantum mechanical/molecular mechanical dynamics. *J. Phys. Chem. B* **2009**, *113*, 3280−3291.

(78) Toniolo, A.; Granucci, G.; Martinez, T. J. Conical Intersections in Solution: A QM/MM Study Using Floating Occupation Semi-empirical Configuration Interaction Wavefunctions. *J. Phys. Chem. A* **2003**, *107*, 3822−3830.
(79) Toniolo, A.; Olsen, S.; Manohar, L.; Martinez, T. J. Conical Intersection Dynamics in Solution: The Chromophore of Green Fluorescent Protein. *Faraday Discuss.* **2004**, *127*, 149−163.
(80) Yamazaki, S.; Kato, S. Locating the lowest free-energy point on conical intersection in polar solvent: Reference interaction site model self-consistent field study of ethylene and CH2NH2+. *J. Chem. Phys.* **2005**, *123*, 114510.
(81) Mori, T.; Nakano, K.; Kato, S. Conical intersections of free energy surfaces in solution: effect of electron correlation on a protonated Schiff base in methanol solution. *J. Chem. Phys.* **2010**, *133*, 064107.
(82) Cui, G.; Yang, W. Conical intersections in solution: Formulation, algorithm, and implementation with combined quantum mechanics/molecular mechanics method. *J. Chem. Phys.* **2011**, *134*, 204115.
(83) Muñoz Losa, A.; Martín, M.; Galván, I.; Aguilar, M. Location of conical intersections in solution using a sequential quantum mechanics/molecular dynamics method. *Chem. Phys. Lett.* **2007**, *443*, 76−81.